Journal of Power Sources 396 (2018) 207–212

Contents lists available at ScienceDirect

Journal of Power Sources

journal homepage: www.elsevier.com/locate/jpowsour

# Internal resistance mapping preparation to optimize electrode thickness and density using symmetric cell for high-performance lithium-ion batteries and capacitors

Kazuaki Kisu[a,b], Shintaro Aoyagi[a], Haruka Nagatomo[a], Etsuro Iwama[a,b,**], McMahon Thomas Homer Reid[a,b], Wako Naoi[b], Katsuhiko Naoi[a,b,c,d,*]

[a] Department of Applied Chemistry, Tokyo University of Agriculture & Technology, 2-24-16 Naka-cho, Koganei, Tokyo 184-8588, Japan
[b] Institute of Global Innovation Research, Tokyo University of Agriculture and Technology, 2-24-16 Naka-cho, Koganei, Tokyo 184-8588, Japan
[c] Division of Art and Innovative Technologies, K & W Inc, 1-3-16-901 Higashi, Kunitachi, Tokyo 186-0002, Japan
[d] Advanced Capacitor Research Center, Tokyo University of Agriculture & Technology, 2-24-16 Naka-cho, Koganei, Tokyo 184-8588, Japan

## HIGHLIGHTS

- An internal resistance prediction map was proposed for LIB electrode optimization.
- New cell design—the counter-electrode-removable symmetric cell— was also proposed.
- Internal resistances were analyzed applying EIS on newly-designed symmetric cells.
- Empirical formula between $R_{ct}$ and electrode density was deduced from EIS analysis. .

## ARTICLE INFO

*Keywords:*
Lithium-ion batteries
Internal resistance
Composite electrode
Symmetric cell
Electrode density

## ABSTRACT

Methods for characterizing and optimizing the internal resistance of electrodes are crucial for achieving the simultaneous goals of high energy density and high power density in lithium-ion batteries. In this study we propose—and confirm the efficacy of—a method for electrode design optimization based on the construction of an *internal resistance map*, a visualization tool for minimizing electrode resistance. The construction of the map proceeds by identifying the three primary components of the electrode resistance—charge-transfer resistance, ionic resistance, and contact resistance—and elucidating the dependence of each component on electrode density and thickness. We fabricate electrode sheets of various densities and thicknesses and conduct electrode impedance spectroscopy (EIS) measurements to measure the dependence of internal resistance on density and thickness, which we characterize via empirical formulas incorporated into our internal resistance map. Using our map, we predict that the resistance per unit area of a nickel-cobalt- manganese (NCM) electrode attains its minimum value at thickness 70 μm and density 2.9 g $cm^{-3}$. We then further use the map to predict variations in IR drop for NCM electrodes of different densities, obtaining results in excellent agreement with experimental measurements.

## 1. Introduction

Efforts to design more sustainable societies have spurred widespread adoption of renewable energy technologies, a trend which is increasingly restructuring fossil-fuel-dependent industrial sectors such as the automobile and heavy-equipment industries [1]. In particular, major nations such as India, France, and England have announced plans to ban the sale of gasoline vehicles within the next few decades, stimulating efforts to accelerate the transition to more environmentally-friendly options such as electric vehicles (EVs), fuel-cell vehicles (FCVs), and plug-in hybrid vehicles (PHEVs) [2]. However, the lithium-ion secondary batteries that supply the driving energy for electric vehicles continue to exhibit significant unrealized potential compared to gasoline, and the need to improve the performance of these devices—particularly in areas such as energy density, power density, and safety—has become an increasingly urgent challenge. Although it is

* Corresponding author. Department of Applied Chemistry, Tokyo University of Agriculture & Technology, 2Naka-cho, Koganei, Tokyo 184-8588, Japan.
** Corresponding author. Institute of Global Innovation Research, Tokyo University of Agriculture and Technology, 2-24-16 Naka-cho, Koganei, Tokyo 184-8588, Japan.
*E-mail address:* k-naoi@cc.tuat.ac.jp (K. Naoi).

https://doi.org/10.1016/j.jpowsour.2018.05.083
Received 11 April 2018; Received in revised form 22 May 2018; Accepted 27 May 2018
0378-7753/ 

generally understood that a tradeoff exists between energy density and power density, recent years have witnessed active research initiatives targeting simultaneous improvements in both of these quantities, focusing primarily on optimizing the design of cells and electrodes to extract maximum performance from the active materials used to construct electrodes. In particular, the design of electrodes—which ultimately determines the speed and quantity of lithium storage—is one factor that directly impacts the energy and power density of cells, and has thus become a focus of intense effort in both research and development settings [3]. The most common technique for designing high-energy-density electrodes is to increase the quantity of active material per unit area; however, this tends to degrade power density—a consequence generally attributed to increased internal resistance and/or reduced ion diffusivity in composite electrodes as the density or the thickness is increased [4,5]. For this reason, the design of electrodes to achieve desired performance benchmarks is a delicate balancing act requiring a creative combination of strategies. In addition, many applications—including HEVs and batteries for renewable-energy-based electric power generation—require high peak speeds for charge and discharge, further emphasizing the urgent need to elucidate the relationship between electrode structure and electrode internal resistance [6]. However, to date most work on electrode design and internal-resistance optimization has proceeded largely by trial and error, employing simple empirical methods with a heavy reliance on knowhow and guesswork. Moreover, optimal electrode structures differ for each possible choice of electrode material [7]. Clearly, the field is in dire need of common, standardized methods of characterization to improve the efficiency of electrode structure design optimization. In this paper, we take a major step in this direction by proposing a new general-purpose method for understanding the relationship between the structure and internal resistance of electrodes; as an immediate byproduct of our novel approach, we use the new understanding it offers to construct an *internal resistance map* that serves as a powerful tool for rationalizing and accelerating the electrode-design process.

To date there have been several reports of studies investigating the relationship between electrode mass and internal resistance with an emphasis on electrode thickness [8,9]. Ogihara et al. used symmetric cells to characterize the internal resistance of electrodes of varying thickness and fixed electrode density *via* electrochemical impedance spectroscopy (EIS) measurements; this analysis successfully isolated the primary components of the electrode resistance—namely, the charge-transfer resistance and the ionic resistance in the pores—on the basis of the following equations, derived from the EIS results and a transmission-line model of cylindrical pores [8,10]:

$$Z_{nonfaradic} = \sqrt{\frac{R_{ion,L}}{2\pi r\ j\omega C_{dl,A}}}\ coth\sqrt{R_{ion,L}\ \ j\omega C_{dl,A}\ \ 2\pi r}\ L$$

$$Z_{faradic} = \sqrt{\frac{R_{ion,L}\ R_{ct,A}}{2\pi r\ (1 + j\omega R_{ct,A}\ C_{dl,A})}}\ coth\sqrt{\frac{R_{ion,L}\ (1 + j\omega R_{ct,A}\ C_{dl,A})\ 2\pi r}{R_{ct,A}}}\ L$$

Ogihara et al. also demonstrated that the two components of the internal electrode resistance (charge-transfer and ionic resistance) are respectively proportional and inversely proportional to the thickness, i.e.

$$R_{ion} = R_{ion,L} \times \frac{L}{n} = k_{ion,T} \times L \quad (1)$$

$$R_{ct} = \frac{R_{ct,A}}{2\pi rL} = k_{ct,T} \times \frac{1}{L} \quad (2)$$

here $L$ and $n$ are the electrode thickness and the number of pores per unit electrode surface area and $k_{ion,T}$, $k_{ct,T}$ are constant coefficients.

On the other hand, the effect of electrode *density* on the relationship between electrode mass and internal resistance has not been adequately characterized to date. Possible reasons for this include **(1)** previous studies have not attempted to optimize the performance of high-density electrodes under high-power conditions, **(2)** it is difficult to fabricate prototype electrodes in research settings (that is, it is difficult to fabricate electrodes of different densities while retaining a constant thickness). Singh et al. fabricated electrodes of various density (porosity) and studied the relationship between electrode density and rate performance; they showed that charge/discharge speeds increase with increasing porosity, while lowering the porosity below a certain threshold value results in a sudden drop in power density [11]. However, studies of this sort have yielded only qualitative conclusions, falling short of providing quantitative insight into the components of the internal resistance. In this study, we fabricate electrodes of various electrode densities at a fixed electrode thickness and use EIS analysis, with data fitted to a transmission-line model [12] [13], to achieve quantitative analysis of internal resistance and isolation of resistance components. In analyzing internal resistance, we use a symmetric cell to eliminate the influence of counter electrodes or reference electrodes [8,10] [14]. Using this cell allows us to avoid contaminating our results with contributions from spurious resistance components, facilitating accurate separation of the resistance of the symmetric electrodes [15]. In previous methods, state of charge (SOC) adjustments for symmetric cells involved a multi-stage process—constructing the full cell, adjusting SOC, deconstructing the full cell, cutting the electrodes, and reconstructing the symmetric cell—which required careful engineering to prevent increases in internal resistance incurred in this process. In this study, we avoid this multi-stage procedure by introducing an original new symmetric-cell design—which we term the *counter-electrode-removable symmetric cell* (CER-SC)—that allows easy insertion and removal of the counter electrode, enabling EIS measurements at varying SOC with no need to deconstruct the cell.

## 2. Experimental

### 2.1. Electrode preparation

Positive electrodes were constructed by preparing a slurry consisting of a 91.0/4.5/4.5 mixture of the active material (NCM electrode: $LiNi_{0.33}Co_{0.33}Mn_{0.33}O_2$, Nippon Chemical Industrial Inc.), a conducting agent (acetylene black: DENKA BLACK HS-100, Denka Company Limited), and a binder (PVDF: KF polymer #1120, KUREHA CORPORATION); this was applied as a coating to a current collector (primer coated foil: Nippon Graphite), subjected to preliminary drying at 60 °C for 3 h, then subjected to primary drying at 80 °C for at least 12 h. To fabricate electrodes of fixed thickness and varying density, we used a Baker film applicator (TESTER SANGYO CO,. LTD) to construct electrodes of varying masses. To control the electrode density, we performed pressing in a roll press to yield electrodes of constant thickness (50 μm) and various masses.

### 2.2. Symmetric cell assembly and electrochemical characterizations

All electrochemical characterizations were carried out using coin cells or laminate cells constructed in a dry room (dew point −40 °C). Impedance measurements were carried out using the cell shown in Fig. 1. For electrochemical experiments, we used an electrolyte (1.0 M $LiPF_6$ EC/DEC, 50/50 vol ratio) and a separator (CELLGUARD2400). The electrodes to be measured were arranged to face each other in a planar configuration and a counter electrode with lithium affixed to both surfaces was inserted between them. To adjust the working electrode SOC, the two working-electrode terminals were shorted together and used as a cathode, while the center lithium electrode was used as an anode; charging and discharging were performed in this half-cell to achieve the desired SOC. Prior to EIS measurements, charge-discharge tests were conducted for NCM electrodes using Li metal counter-electrodes placed in the center of a CER-SC cell, and the potential at 50% SOC was determined based on the slopes of the resulting charge/discharge curves for NCM electrodes. After achieving the desired SOC,

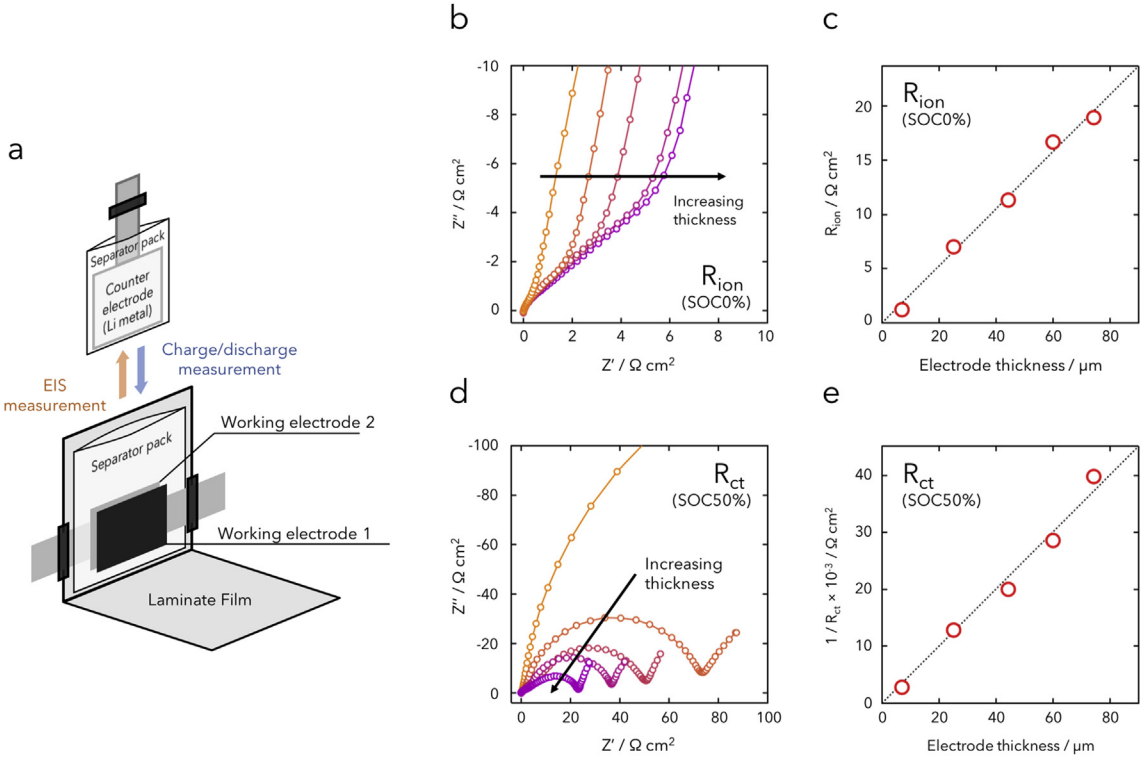


**Fig. 1.** (a) Cell configuration of counter electrode removable symmetric cell for EIS measurements, (b) Nyquist plots for symmetric cells using two identical positive electrodes at 25 °C on electrode thickness for electrodes prepared at SOC0%, (c) Summary of relationship between $R_{ion}$ and electrode thickness, (d) Nyquist plots at 25 °C on electrode thickness for electrodes prepared at SOC50%, (e) Summary of relationship between $R_{ct}$ and electrode thickness.

we removed the lithium metal in a dry room to obtain a two-electrode symmetric cell. AC impedance measurements were performed under open-circuit conditions using Solartron Modulab. EIS measurements were conducted at a fixed room temperature of 25 °C and an amplitude of 10 mV with the frequency varied from 1 MHz to 1 Hz. For data fitting, the equivalent circuit for impedance spectra at the SOC 0% and SOC 50% used the generalized finite length Warburg element open-circuit terminus (Wo) and short-circuit terminus (Ws) for descriptive purposes, respectively [16]. To focus on ionic resistance and charge transfer resistance, the value of real Z (imaginary Z is zero) is normalized as zero in Nyquist plots obtained by EIS measurements.

## 3. Results and discussion

### 3.1. Using the simple symmetric cell to investigate the thickness dependence of internal resistance components ($R_{ct}$, $R_{ion}$)

In this study, we use the counter-electrode-removable symmetric cell (CER-SC) of Fig. 1a to make accurate EIS measurements of electrodes at varying SOC, separating the contributions of ionic resistance and charge-transfer resistance. We begin by verifying that our CER-SC setup yields accurate measurements of internal resistance components by using it to reproduce results reported in previous papers. Thus, following Ogihara et al. [8], we analyze the internal resistance ($R_{ion}$ and $R_{ct}$) of electrodes of various thicknesses (ranging from 10 μm to 150 μm) with the electrode density held fixed. Fig. 1b shows Nyquist plots at SOC = 0%. For all electrodes, independent of thickness, we observe a resistance component with a 45° slope in the high-frequency regime. From equation (1) we identify this 45° slope component as $R_{ion}$ [17]. The relationship between electrode thickness and $R_{ion}$ is shown in Fig. 1c; from this figure we see that $R_{ion}$ is proportional to thickness. This agrees with the relationship reported by Ogihara et al. confirming the accuracy of our EIS measurements at SOC = 0%.

Fig. 1d shows Nyquist plots at SOC = 50%. For all electrodes, independent of thickness, we observe a resistance component forming a semicircle in the high-frequency regime. From equation (2) we identify this component as arising from $R_{ct}$. The relationship between electrode thickness and $R_{ct}$ is shown in Fig. 1c; from this figure we see that $R_{ct}$ is inversely proportional to thickness, again in agreement with results reported by Ogihara et al. These findings demonstrate that EIS measurements using our CER-SC may be used effectively to analyze the internal resistance of electrodes.

### 3.2. Dependence on electrode density and internal resistance ($R_{ct}$, $R_{ion}$, $R_{con}$)

Figure S1 shows pore distributions, as measured via mercury porosimetry for electrodes with densities and thicknesses controlled by roll pressing (densities {2.7, 2.9, 3.4} g cm$^{-3}$). Note that the pore volume decreases as the density increases (i.e. as the porosity decreases); at the same time, we see that the pores themselves become smaller. This finding is similar to results reported by Kitada et al. suggesting that the trend observed here is a general phenomenon: as pores are crushed in the process of increasing the density, the pores in the interior of the hybrid electrode are uniformly compressed [18]. In view of this result, the relation between electrode density and pore radius may be expressed as follows.

$$\phi = 1 - \frac{\rho_{real}}{\rho_{theoretical}}$$

$$Lr^2\pi = \phi V$$

$$r = \left(\frac{\phi V}{L\pi}\right)^{\frac{1}{2}}$$

here $\phi$ is the porosity, $\rho_{real}$ is the electrode density, $\rho_{theoretical}$ is the theoretical electrode density, and $V$ is the volume of the electrode. Combining this relation with equation (1) relating $R_{ion}$ to $L$ and $r$ allows

us to express the relationship between $R_{ion}$ and density in the form

$$R_{ion} = \frac{\varrho}{\pi r^2} \times \frac{L}{n} \quad \text{(1)original equation}$$

$$R_{ion} = \frac{\varrho L}{A\phi} = k_{ion,D} \times \frac{1}{\phi} = \frac{k_{ion,D}}{\left(1 - \frac{\rho_{real}}{\rho_{theoretical}}\right)} \tag{3}$$

where $\varrho$ is the specific capacity and $k_{ion,D}$ is a proportionality constant relating ionic resistance to electrode density. This equation shows that the relationship between density and $R_{ion}$ is not a simple proportionality; instead, the resistance increases dramatically as the density approaches the theoretical density. On the other hand, on theoretical grounds we expect $R_{ct}$ to be independent of electrode density and inversely proportional to electrode mass (Equation (2)). We will use the following functional form to describe the relationship between density and $R_{ct}$:

$$\rho_{real} = \frac{W}{V}$$

$$A = a \times W$$

$$R_{ct} = \frac{R_{ct,A}}{A} = \frac{R_{ct,A}}{a \times V \times \rho_{real}} = k_{ct,D} \times \frac{1}{\rho_{real}} \tag{4}$$

here $W$ is the electrode mass, $A$ is the surface area of the active material within the electrode, $a$ is a proportionality constant relating $A$ to $W$, and $k_{ion,D}$ is a proportionality constant relating the charge-transfer resistance to the electrode density. In the remainder of our analysis we will assume the validity of equations (3) and (4).

### 3.3. Dependence of internal resistance on density (porosity)

Fig. 2a shows Nyquist plots obtained for electrodes of various densities using our CER-SC cell at SOC = 0%. We see that all electrodes exhibit a resistance component with typical slope 45°, which corresponds within the transmission-line model to ionic resistance in the electrode interior. Note that this ionic resistance increases significantly with increasing density. This clearly demonstrates that internal resistance of electrodes is not determined solely by the membrane-thickness effects observed by Ogihara et al., but also by electrode density. Fig. 2b shows the resistance components obtained by fitting the Nyquist data to a power-law functional form. Note that the rate at which the ionic resistance increases with electrode density is nonlinear, varying like an $n^{th}$-degree polynomial. The dashed curve in Fig. 2b shows the results of fitting to the form of equation (3). The successful fit indicates that equation (3) accurately describes the relationship between electrode density and $R_{ion}$. Increasing the electrode density has the effect of reducing pore sizes and narrowing the pathways for ion transport through the electrode, resulting in increased resistance.

Next, Fig. 2c shows Nyquist plots for electrodes of various densities at SOC = 50%. We see that the typical semicircular curve due to charge-transfer resistance is visible in all plots. Note that the semicircles decrease in size as the electrode density increases, an effect that may be attributed to increased electrode mass. Fig. 2d shows the relationship between the electrode density and the value of $R_{ct}$ obtained by fitting the semicircular portions of the data curves. We see that the relationship between electrode density and $R_{ct}$ obtained in this way is not described by the simple inverse-proportionality relation of equation (4). Empirical formulas obtained by fitting our experimental data indicate that the relation between $R_{ct}$ and the density is a power law:

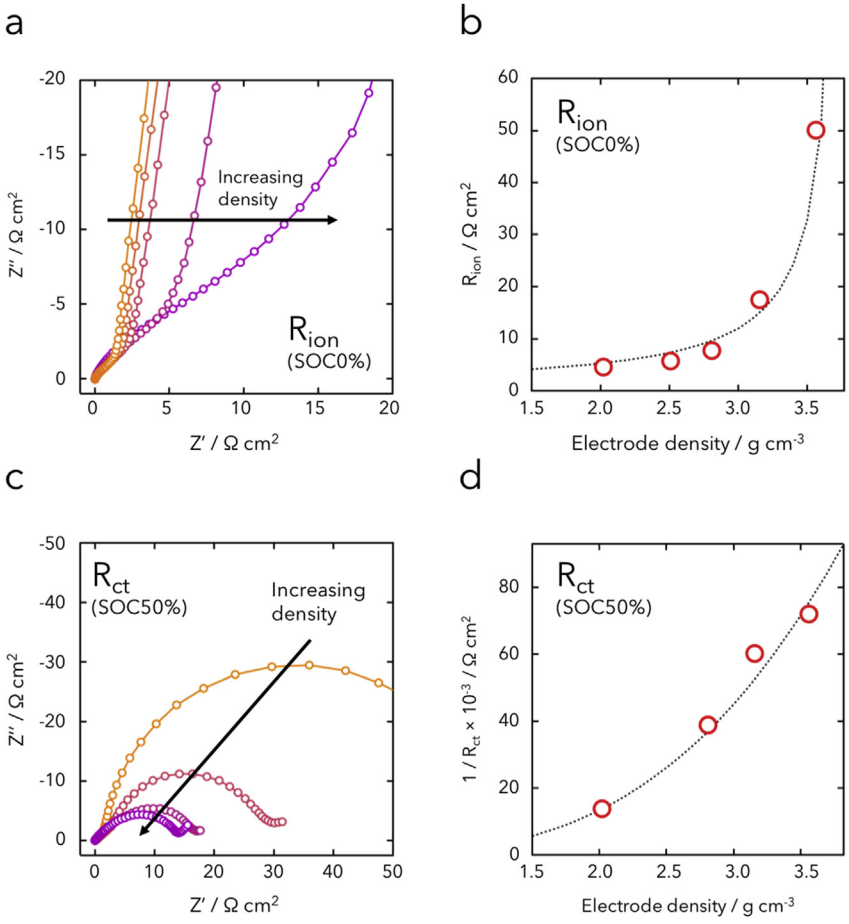


**Fig. 2.** (a) Nyquist plots for symmetric cells using two identical positive electrodes at 25 °C on electrode density for electrodes prepared at SOC0%, (c) Summary of relationship between $R_{ion}$ and electrode density, (d) Nyquist plots at 25 °C on electrode density for electrodes prepared at SOC50%, (e) Summary of relationship between $R_{ct}$ and electrode density.

$$R_{ct} = k_{ct,D} \times \left(\frac{1}{\rho_{real}}\right)^{n} \quad (5)$$

here $n$ is a coefficient used for fitting purposes which takes a value of approximately $n \approx 3$ in our calculations. We are currently investigating the chemical significance of this value, which we believe to arise from changes in volume within the electrode. We expect that charge-transfer reactions occur at regions within the electrode corresponding to interfaces at which three phases (active material, carbon conducting agents, and electrolyte) are simultaneously present. Thus, we conclude that the total surface area of these three-phase interfacial regions increases in proportion to the volume within the electrode.

In typical electrodes, high-resistance components commonly arise in low-density configurations; this is due to contact resistance ($R_{con}$) between the electrode current collector and the active material or conducting agent [19]. To observe this contact resistance, we use a current collector that is *not* carbon-coated and measure its contact resistance under low-density conditions (Fig. S2). Fitting the resulting Nyquist plot, including its semicircular portion, and computing $R_{con}$ yields the results summarized in Fig. S2b. From the plot of $R_{con}$ vs. electrode density thus obtained we derive the following empirical formula.

$$R_{con} = k_{con,D} \times \frac{1}{\rho_{real}^{n}} \quad (6)$$

here $n$ is a coefficient used for fitting purposes which takes a value of approximately $n \approx 3$ in our calculations. We are currently investigating the chemical significance of this value, which may vary depending on the precise conditions of the current collector and other conditions.

### 3.4. Using internal-resistance formulas to create a tool for rationalizing and accelerating electrode design

Combining the formulas relating internal resistance to thickness [equations (1) and (2)] with the formulas relating internal resistance to electrode density [equations (3), (5) and (6)] yields an *internal resistance map* that serves as a valuable tool for electrode design. By using these formulas together with measurements of $R_{ion}$ and $R_{ct}$ at arbitrary values of the electrode density and thickness, it becomes possible to predict both individual resistance components and the overall resistance of many different electrode structures. Fig. 3a shows the electrode resistance map determined by equations (1)–(3) and (5) and (6); in this figure, the $X$ and $Y$ axes respectively indicate thickness and electrode density, while color values indicate total resistance. The darkest blue regions of the graph correspond to the lowest-resistance electrode designs. Because the two primary resistance components vary with thickness in opposite ways—namely, $R_{ct}$ decreases and $R_{ion}$ increases with increasing thickness—the resistance attains a minimum at a certain critical thickness. Similarly, $R_{con}$ decreases and $R_{ion}$ increases with increasing density, giving rise to a resistance minimum at a particular critical density. These factors explain why the resistance attains a minimum at certain points within the two-dimensional plane of the map. Based on the map of Fig. 3a, we expect the resistance per unit area to be minimized for an electrode of thickness 70 μm and density 2.9 g cm$^{-3}$, We also find that the minimal resistance components obtained for a given electrode mass (support line in Fig. 3a) tend to shift in the direction of lower density as the electrode mass increases. This is because, as the mass increases, the contributions of the contact resistance—which depends only on density—and of $R_{ion}$, which depends on both density and thickness, become more significant. To assess the usefulness of our internal resistance map as a tool for accelerating electrode design, we studied trends in the DC resistance of electrodes as the density is varied. Fig. 3b shows discharge curves at same current density for electrodes of varying densities. Considering the behavior immediately after the onset of current flow, we find a large overvoltage ΔV in both the low-density and high-density regimes. In Fig. 3c we have plotted experimental values of ΔV (filled circles) against the curve predicted by our electrode-design assistance tool (dashed curve). The excellent agreement between measured data and the predictions of our tool demonstrate its effectiveness in rationalizing and accelerating the process of electrode design.

## 4. Conclusion

In this study we introduced a new cell design—the counter-electrode-removable symmetric cell (CER-SC)—and a transmission-line model to study the relationship between electrode density and internal resistance. Using our new cell to conduct EIS analysis of electrodes of varying thickness yielded results in agreement with previous reports, confirming the efficacy of our CER-SC for electrode resistance analysis. Based on measurements of various electrodes using a mercury porosimeter, we observed the dependence of the density on the electrode pore radius and obtained a formula relating $R_{ion}$ to electrode density.

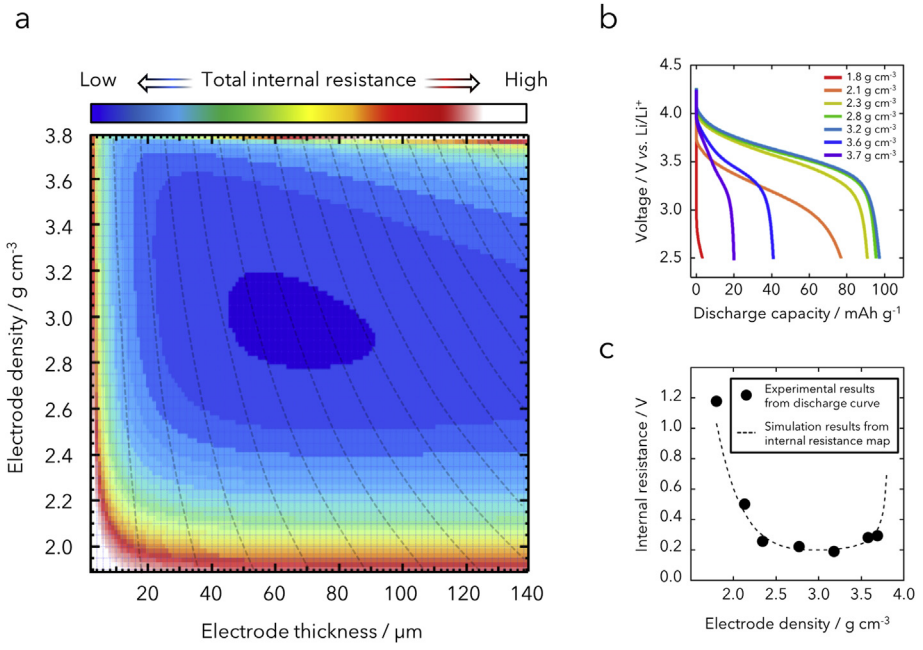


**Fig. 3.** (a) An internal resistance mapping to optimize electrode thickness and density using symmetric cell, (b) Discharge curve using different electrode density from 1.8 to 3.8 g cm$^{-3}$ at same current density, (c) Relationship between experimental internal resistance (IR drop calculated from Fig. 3 b) and simulated internal resistance (expected result by internal resistance mapping from Fig. 3 a).

Considering the increase in $R_{ion}$ due to **(1)** the mass increase associated with increased electrode density and **(2)** the mass increase due to increasing electrode thickness, our results indicated that effect **(1)** is greater than effect **(2).** On the other hand, the dependence of $R_{ct}$ on electrode density arises not only from the simple dependence on the surface area of the active electrode material, but also from a dependence on the electrode density itself. In addition to the formulas we obtained relating internal electrode resistance components ($R_{ct}$, $R_{ion}$, and $R_{con}$) to electrode density, we combined these formulas with formulas relating internal resistance components ($R_{ct}$ and $R_{ion}$) to thickness to obtain an *internal resistance map,* a tool that facilitates electrode design by predicting resistance components of electrode materials. Values of the internal electrode resistance predicted by our map are in approximate agreement with values obtained from ΔV measurements in charge/discharge experiments, demonstrating the usefulness of our map as a tool for assisting the process of electrode design. We are hopeful that the new tools we have introduced will enable high-accuracy design of electrodes such for batteries and even electrochemical capacitors with greater ease and efficiency than were previously possible.

## Acknowledgement

This study was supported by JSPS KAKENHI Grant Numbers JP25249140, JP17K05962, JP16K17970, JP17K14920, and the Center of Innovation Program from Japan Science and Technology Agency (A-STEP; AS282S002d).

## Appendix A. Supplementary data

Supplementary data related to this article can be found at http://dx.doi.org/10.1016/j.jpowsour.2018.05.083.

## References

[1] D. Larcher, J.M. Tarascon, Nat. Chem. 7 (2015) 19–29.
[2] M. Berecibar, I. Gandiaga, I. Villarreal, N. Omar, J. Van Mierlo, P. Van den Bossche, Renew. Sustain. Energy Rev. 56 (2016) 572–587.
[3] J. Ye, A.C. Baumgaertel, Y.M. Wang, J. Biener, M.M. Biener, ACS Nano 9 (2015) 2194–2202.
[4] H. Zheng, J. Li, X. Song, G. Liu, V.S. Battaglia, Electrochim. Acta. 71 (2012) 258–265.
[5] T. Danner, M. Singh, S. Hein, J. Kaiser, H. Hahn, A. Latz, J. Power Sources 334 (2016) 191–201.
[6] B. Wang, J. Xu, B.G. Cao, X. Zhou, J. Power Sources 281 (2015) 432–443.
[7] S. Ha, V.K. Ramani, W. Lu, J. Prakash, Electrochim. Acta. 191 (2016) 173–182.
[8] N. Ogihara, Y. Itou, T. Sasaki, Y. Takeuchi, J. Phys. Chem. C 119 (2015) 4612–4619.
[9] R. Zhao, J. Liu, J. Gu, Appl. Energy 139 (2015) 220–229.
[10] N. Ogihara, S. Kawauchi, C. Okuda, Y. Itou, Y. Takeuchi, Y. Ukyo, J. Electrochem. Soc. 159 (2012) A1034–A1039.
[11] M. Singh, J. Kaiser, H. Hahn, Batteries 2 (2016) 35.
[12] R. de Levie, Electrochim. Acta. 8 (1963) 751–780.
[13] M. Itagaki, S. Suzuki, I. Shitanda, K. Watanabe, Electrochemistry 75 (2007) 649–655.
[14] C.H. Chen, J. Liu, K. Amine, J. Power Sources 96 (2001) 321–328.
[15] C. œLim, B. Yan, H. Kang, Z. Song, W.C. Lee, V. De Andrade, F. De Carlo, L. Yin, Y. Kim, L. Zhu, J. Power Sources 328 (2016) 46–55.
[16] W. Sugimoto, H. Iwata, K. Yokoshima, Y. Murakami, Y. Takasu, J. Phys. Chem. B 109 (2005) 7330–7338.
[17] D. Cericola, M.E. Spahr, Electrochim. Acta. 191 (2016) 558–566.
[18] K. Kitada, H. Murayama, K. Fukuda, H. Arai, Y. Uchimoto, Z. Ogumi, E. Matsubara, J. Power Sources 301 (2016) 11–17.
[19] C. Portet, P.L. Taberna, P. Simon, C. Laberty-Robert, Electrochim. Acta. 49 (2004) 905–912.